Journal of Process Control 135 (2024) 103150

Contents lists available at ScienceDirect

Journal of Process Control

journal homepage: www.elsevier.com/locate/jprocont

Optimal control of viscous fingering

Nicolas Petit

MINES Paris, PSL University Centre Automatique et Systèmes, 60, bd Saint-Michel, 75272, Paris, France

ARTICLE INFO

Keywords:
Microfluidics
Control of micro- and nano-systems
Non-smooth optimal control problems
Hele-Shaw cell
Distributed parameters systems

ABSTRACT

The paper considers the problem of optimally filling a Hele-Shaw cell. The system is subject to viscous fingering effect. It is shown that, despite the threshold terms appearing on the right-hand side of the governing equations, the dynamics can be rewritten using several prime integrals. This allows reforming optimal control problems for the Fourier modes describing the fluid interface into smooth optimization problems, in the sense of Gâteaux derivative. Some numerical experiments illustrate the advantages of using the optimal solutions obtained using this reformulation instead of the currently known time-dependent injection rates.

1. Introduction

The viscous fingering effect occurs in numerous fields of science and engineering ranging from microfluidics, chromatographic separation, adhesion [1], to geological processes for enhanced oil recovery [2], or CO2 sequestration in porous media [3,4], among others. This effect is observed at the interface between fluids having different viscosities. In general, when a less viscous fluid displaces a more viscous fluid, the boundary between the two fluids gradually deforms and acquires a visually remarkable geometry, described as “fingers”.

At a laboratory scale, the phenomenon is easily observed in a Hele-Shaw cell using air and water as fluids. A Stokes flow is created between two parallel flat plates separated by a very small gap. The gap is initially filled with a viscous fluid (water). In the center of the cell, a less viscous fluid (air) is injected through a tiny hole in the top plate. While the injected fluid initially retains a circular shape, it soon develops into radial fingers, sometimes fractal patterns [5], as the radius of the interface increases, see illustration in Fig. 1. The difference of viscosities is the root cause for the phenomenon described as Saffman–Taylor hydrodynamic instability at the fluid–fluid interface [6]. In the pioneering works of [7,8], a linear stability analysis explains how surface tension fails to suppress the growth of small perturbations at the fluid–fluid interface as the interface radius increases.

In addition to laboratory experiments, numerous numerical studies of the governing partial differential equations have allowed the reproduction of the nonlinear evolution of the fingering shapes. A problem of practical and theoretical interest is to control the shape of the interface. Mitigating instability would have strong potential applications, such as the efficient loading and unloading of underground porous media and reservoirs in the energy industry. So far, several attempts of active control of the interface have been made, considering various actuation possibilities. For example, in [9] a force is exerted on the top plate. In [10], a position controller on the bottom plate is used to control the gap thickness as a function of time. This paper explores another strategy employing time-varying flowrates. This path has been identified by many researchers and investigated experimentally with success [10–12] and references therein. It is quite straightforward to implement using pressure-based flow controllers, as is common practice in microfluidics.

The governing equations of the viscous fingering effect under time-varying flowrates are well known but not so easy to handle from a control theory perspective. The shape of interface is described using a (truncated) Fourier series. Because of the geometric expansion of the boundary, the modes equations are in fact time-varying. While all the modes have contracting behaviors at first, they eventually all become unstable as the boundary grows. When a mode becomes unstable, its random initial condition leads to the development of a number of “fingers”, see [13]. The transient between the contracting behavior to the expansion is modeled using `max` functions used as thresholds terms in the right hand-side of the governing differential equations. The single control variable has to be used to control many (typically 10 to 30) variables. It appears in the equation of every mode. Each jump occurs at an instant that is influenced by the history of the control variable.

Among the various control problems one could study, the literature has considered the formulation of an optimal control problem (OCP) over a finite time-horizon, a mathematical transcription of the following practical problem “*if one wishes to inject a certain amount of fluid in a given time, what would be the optimal time-dependent injection rate for which the perturbation amplitudes could be truly minimized?*” [14]. Many heuristic have been tested, e.g. sinusoids [15], piece-wise constant flowrates [16] or inversely proportional to the average radius [11].

Interestingly, at the expense of several drastic simplifications, the OCP can be solved analytically. Following [13], it is possible to identify

E-mail address: nicolas.petit@minesparis.psl.eu.

https://doi.org/10.1016/j.jprocont.2023.103150
Received 29 September 2023; Received in revised form 4 December 2023; Accepted 18 December 2023

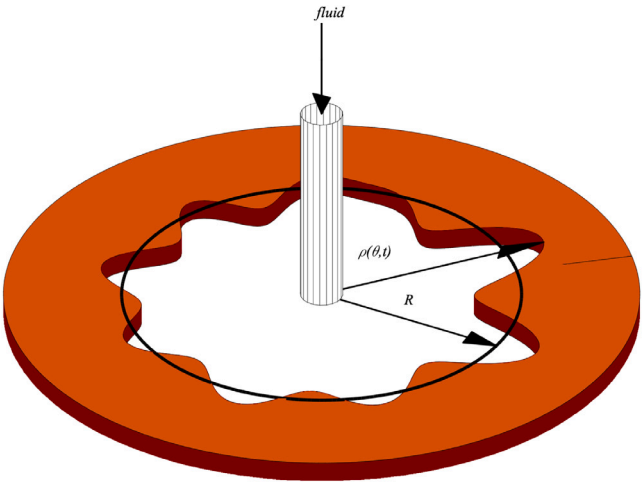

Fig. 1. Hele-Shaw cell. A less viscous fluid is radially injected into a more viscous fluid contained into two parallel plates. Illustration inspired by [10].

at each instant the fastest growing (or most unstable) mode. Considering only this mode over the whole time horizon, [14] has been able to formulate a single-input single-output (SISO) dynamics with an integral cost to be minimized. Surprisingly, the associated Euler–Lagrange equation boils to a (very) simple differential equation, having a closed-form solution, stating that the average radius should simply grow linearly with time. In turn, the flowrate should follow a time-affine law, which expression is readily solved. This remarkable result has spurred a large interest in the community, and numerous numerical and experimental validation have shown the robustness of the approach [12,17].

The present article wishes to show that the simplifications of [14] are not necessary and that some performance improvement can be obtained by solving the OCP in its original formulation, i.e. with all the modes at once.

Mathematically, the OCP has some apparent singularities in its formulation. Because of the threshold effects, the trajectories of the modes are defined over nested intervals. Each starting time depends on the control history, in an implicit manner described by an integral equation. In the article it is shown that, despite these singularity terms, the problem is in fact smooth. The jumps can be simply recast as input-dependent delays, which are ordered. Then, several calculus stress that the differential equations have some prime integrals. This allows one to propose a compact reformulation of OCPs with a general L2-norm functional. Following [18], the Gâteaux differentiability of the cost functional is established. A necessary condition for any local extremal is that the Gâteaux derivative should be zero in all admissible directions, making it a critical point. This allows one to use any descent method to determine an optimal solution. The feasibility of the optimization procedure and the performance improvement are numerically illustrated on a test-case from the literature.

The paper is organized as follows. Section 2 recalls the model of the Hele-Shaw cell, and formulates a L2-norm OCP of practical interest. Prime integrals are introduced to reformulate the OCP into a multiple stage continuous time problem. Smoothness of this formulation is established in Section 3. Numerical results are reported in Section 4. Conclusions and perspectives are given in Section 5.

Notations

Let $T > 0$, we note $C^1([0,\, T], \mathbb{R})$ the class of C^1 functions from $[0,\, T]$ to $\mathbb{R}$.

2. Model of the Hele-Shaw cell

Viscous fingering in Hele-Shaw cells has been the subject of strong focus among the applied mathematics, physics and biology communities for many years [12]. A Hele-Shaw cell is an experimental device consisting of two parallel plates separated by a small gap filled with viscous fluid.[1] At the center of the device, an inviscid (or less viscous) fluid is injected through a hole in one the plates. At the interface between the two fluids, some patterns gradually develop as the injection continues. Because of their appearance, the patterns are named "fingers". The root cause of the viscous fingering effect is the Saffman–Taylor instability [6]. In the early stage of the development, the fingers are relatively wide and not very numerous. Later on, if nothing is done, branching and tip-splitting occur, rendering the shape of the interface fractal.[2]

This paper focuses on the early mitigation of viscous fingering by controlling or limiting the pattern formation. As control mean, the injection rate is considered. The interface is described by a harmonic deposition. The metric under consideration is a L2-norm in the harmonic space, which measures how close to a circle the interface is. This formulation is in accordance with the recent works on the subject [12].

The model assumes that the two fluids are incompressible and immiscible. The viscous fluid is infinite in its extent. Polar coordinates (R, θ) are employed. The classical notations from the literature are used [13]. The interface has a perturbed shape described as

$$\mathcal{R} = R(t) + \xi(\theta, t)$$

where R is the time dependent unperturbed radius. It is an increasing function with a non zero initial condition $R(0) = R_0 > 0$ which guarantees that the system stays away from the singularity of the polar coordinates.

2.1. Model from the literature

2.1.1. Physical description

The interface perturbation amplitude is described in terms of its N first complex Fourier modes

$$\xi(\theta, t) = \sum_{n=-N}^{n=N} \xi_n(t) \exp(in\theta), \qquad \xi_n(t) = \frac{1}{2\pi} \int_0^{2\pi} \xi(\theta, t) \exp(-in\theta) d\theta$$

To guarantee mass conservation, one defines $\xi_0 = -\frac{1}{2R} \sum_{n=1}^{\infty} |\xi_n(t)|^2 + |\xi_{-n}(t)|^2$. Noting $a_n = \xi_n + \xi_{-n}$, $b_n = i(\xi_n - \xi_{-n})$, one has

$$\xi(\theta, t) = \xi_0 + \sum_{n=1}^{n=N} a_n(t) \cos(n\theta) + b_n(t) \sin(n\theta)$$

The viscosities of the two fluids are noted $\eta_1 \ll \eta_2$. The viscosity contrast is defined as

$$A = \frac{\eta_2 - \eta_1}{\eta_1 + \eta_2}$$

The surface tension σ and the distance between the two plates b serve to define the constant parameter

$$\alpha = \frac{b^2 \sigma}{12(\eta_1 + \eta_2)}$$

Note $Q \geq 0$ the injection rate (area covered per unit time). The unperturbed radius is governed, using a volume balance principle, by

$$\frac{d}{dt} R^2(t) = \frac{1}{\pi} Q(t)$$

[1] The gap is much smaller than the scale of variation of the velocity field in a plane parallel to the plates so that the flow is assumed to operate at very low Reynolds numbers [19].

[2] The presence of these fingering is usually considered as undesirable, in all the applications where the purpose of the injection of an inviscid fluid is to put the viscous fluid into motion, usually to recover it, such as in industrial applications in underground porous reservoirs [2].

The Fourier modes are governed by the following equations, stemming from equating modes on each side of Darcy's law [13] which describes that the velocity field is derived from a potential proportional to the pressure (and that the vorticity is null) [19,20],

$$\dot{\xi}_n(t) = \lambda_n(t)\,\xi_n(t) \tag{1}$$

where the linear growth rate is

$$\lambda_n(t) = \frac{1}{2\pi R^2(t)}(A|n| - 1)\left(Q(t) - \frac{2\pi\alpha|n|(|n|+1)}{R(t)}\right)$$

2.1.2. Noise model

From Eq. (1), one directly has the general expression

$$\xi_n(t) = \xi_n(0)\,\exp\left(\int_0^t \lambda_n(s)ds\right)$$

This stresses that if $\int_0^t \lambda_n(s)ds > 0$ the disturbance grows, and otherwise the disturbance is damped. This simple consideration leads to the seminal "Model B" by [21] which represents the solution using

$$\dot{f}_n(t) = \max(0, \lambda_n(t)), \quad f_n(0) = 0$$

and notes

$$\xi_n(t) = \xi_n(0)\,\exp\left(f_n(t)\right) \tag{2}$$

In this model, the process is supposed to be excited by some random noise, represented as a random initial condition $\xi_n(0)$, in accordance with [13] where the randomness lies in the phase of the complex number which is uniformly distributed over $[0, 2\pi]$ while the modulus is set to a constant value. Due to this choice, there is a bijective relationship between the two variables $a_n(t)^2 + b_n(t)^2$ and $f_n(t)$.

2.1.3. Normalization and summary of the model

Note $P(t) = R(t)^2$, $u(t) = \frac{Q(t)}{\pi}$, and consider the system with $A = 1$ (without loss of generality[3]), then the system is governed by, for $n = 2, ..., N$

$$\lambda_n(t) = \frac{n-1}{2P(t)}u(t) - \frac{\alpha\, n(n^2-1)}{P^{3/2}(t)} \tag{4}$$

$$\dot{f}_n(t) = \max(0, \lambda_n(t)), \quad f_n(0) = 0 \tag{5}$$

$$\dot{P} = u, \quad P(0) = R_0^2 \tag{6}$$

This representation is minimal, as $f_0 = 0$, $f_1 = 0$, $f_{-n} = f_n$, $n = 1, ..., N$.

2.2. A problem of interest

In Eq. (2), the mode appears as a linear function of its random initial condition. A natural OCP formulation favoring roundness is thus expressed in terms of the growth factors f_n, $n = 2, ..., N$. We employ a L2-norm.[4] This formulation is independent from the random initial condition. The constraint maintaining the total amount of injected fluid over a given time horizon T is simply a terminal constraint on the unperturbed radius $R(T) = R_T$ where R_T is a given parameter. At all times the flowrate must be non negative. This leads to the following OCP.

[3] This assumption is common in the literature. Relaxing it is not troublesome. Eq. (11) will simply be replaced by

$$f_n(t) - \frac{J_n}{J_2}f_2(t) + \left(\frac{2A-1}{2J_2}J_n - \frac{An-1}{2}\right)\log P(t) \tag{3}$$

with $J_n = n(An-1)(n+1)$, $n = 2, ..., N$. The Eqs. (11) and (3) match for $A = 1$ giving $J_n = I_n$ in this case.

[4] A possibility, without loss of generality, would be to consider a weighted L2-norm, to account for difference in the probability distributions of the initial conditions of the modes.

Problem 1. Note the L2-norm cost function

$$J = \sum_{n=2}^{N}\left(f_n(T)\right)^2 \tag{7}$$

$$\begin{aligned} \underset{u(t)\geq 0,\forall t\in[0,\,T]}{\text{minimize}} \quad & J \\ \text{subject to} \quad & (5), (6), \forall t \in [0,\,T], \\ & P(T) = R_T^2 \end{aligned} \tag{8}$$

Problem 1 is mathematically unusual, due to the "max" function appearing in the right hand-side of Eq. (5). The non differentiability prevents one from applying the classic calculus of variations techniques which assume smooth right-hand sides of differential equations [22]. Fortunately, some calculations allow one to reformulate Problem 1, without the "max" function, using a multiple stage continuous time formulation described next. A first step in the derivation of this new formulation is to compute prime integrals of the dynamics.

2.3. Prime integrals

For each $n = 2, ..., N$, we note

$$t_u^n = \sup\{t,\ \text{s.t. } f_n(t) = 0\} \tag{9}$$

In the sequel, each of these variables is referred to as "growth starting time of mode n". The subscript stresses the (implicit) dependence on the control input.

Once all Eq. (5) evolve in their unsaturated regimes (past the growth starting times), they share some prime integrals. Indeed Eq. (5) gives $\dot{f}_n(t) = \frac{n-1}{2P(t)}\dot{P}(t) - \alpha\frac{I_n}{P^{3/2}}$ which can be rewritten under the form

$$\frac{d}{dt}(f_n - \frac{n-1}{2}\log P) = -\alpha\frac{I_n}{P^{3/2}} \tag{10}$$

with $I_n = n(n^2-1)$. This shows that the system (10) of $(N-1)$ variables has $(N-2)$ invariants. For $n = 3, \dots, N$ the following variables are constant

$$f_n(t) - \frac{I_n}{6}f_2(t) + \left(\frac{I_n}{12} - \frac{n-1}{2}\right)\log P(t) \tag{11}$$

Using Eq. (11) on each interval $[t_u^n, T]$ allows one to rewrite the cost function J in Eq. (7) as

$$J = \sum_{n=2}^{N}\left(\frac{I_n}{6}\left(f_2(T) - f_2(t_u^n)\right) + L_n\,\log P(t_u^n) - 2L_n\,\log R(T)\right)^2$$

with $L_n = \frac{I_n}{12} - \frac{n-1}{2}$. In this expression, $R(T) = R_T$ is constant, which allows one to write

$$J = \sum_{n=2}^{N}\left(F_n\left(f_2(T) - f_2(t_u^n), P(t_u^n)\right)\right)^2 \tag{12}$$

with

$$(x, y) \mapsto F_n(x, y) \triangleq \frac{I_n}{6}x + L_n\log y - 2L_n\log R(T) \tag{13}$$

2.4. Reformulation as a multiple stage continuous time OCP

Under the form (12), it appears that the OCP can be rewritten with only two state variables, $x(t) = f_2(t)$ and $P(t)$, so that the problem to solve is

Problem 2 (*Multiple Stage Optimal Control at Times Dependent on the Control*)**.**

$$\begin{aligned} \underset{u(t)\geq 0,\forall t\in[0,\,T]}{\text{minimize}} \quad & J = \sum_{n=2}^{N}\left(F_n\left(x(T) - x(t_u^n), P(t_u^n)\right)\right)^2 \\ \text{subject to} \quad & \dot{x}(t) = \frac{1}{2P(t)}u(t) - \frac{6\alpha}{P^{3/2}(t)}, \quad x(t_u^2) = 0, \\ & \dot{P}(t) = u(t), \quad P(0) = R_0^2, \\ & P(T) = R_T^2 \end{aligned} \tag{14}$$

where, for $n = 2, ..., N$, F_n is given in Eq. (13) and t_u^n is defined by Eq. (16).

3. Smoothness of the optimal control problem

Compared to Eq. (5), the form (14) does not involve any "max" function. The smoothness can be more directly studied. A first step of the study is to establish the uniqueness and smoothness of the implicitly-defined growth starting times t_u^n, $n \in 2, ..., N$.

Lemma 1. *Consider any input signal of the form* $[0, T] \ni t \mapsto u(t) = u_0 + v(t)$ *where* $u_0 > 0$, $|v| \leq M_0$, $|\dot{v}| \leq M_1$ *satisfying the inequality*

$$\frac{1}{2}(u_0 - M_0)^2 - M_1(u_0 + M_0 T) \geq \ell > 0 \tag{15}$$

for some ℓ. *The growth starting times are uniquely defined, in ascending order* $t_u^2 < t_u^3 ... < t_u^N$, *and Gâteaux differentiable at* u *in any direction* $h \in C^1([0, T], \mathbb{R})$.

Proof. Each t_u^n is implicitly defined by the condition $\lambda_n(t_u^n) = 0$ which, equivalently, gives $u(t_u^n) = \frac{2\alpha n(n+1)}{P^{1/2}(t_u^n)}$ or, more conveniently

$$u^2(t_u^n) \int_0^{t_u^n} u(s)ds = 4\alpha^2 n^2 (n+1)^2 \tag{16}$$

or

$$\frac{d}{dt} R^3(t_u^n) = 3\alpha\, n(n+1)$$

Interestingly, the mapping $t \mapsto \frac{d}{dt} R^3(t) \triangleq W(t)$ can be shown to be monotonic. Indeed, some line of calculus give $\frac{d^2}{dt^2} R^3(t) = \frac{3}{2R(t)} \left(\frac{u^2(t)}{2} + \int_0^t u(s)ds\, \dot{u}(t) \right)$. By integration, under assumption (15), R is strictly positive for all t and upper bounded. The conclusion stems from the assumption (15), which allows to lower-bound $\frac{d^2}{dt^2} R^3 > \frac{3}{2(u_0 + M_0 T)} \ell$.

From this strict monotonicity and the application of the global inversion theorem, one obtains the uniqueness and smoothness of the $t_u^n = W^{-1}(3\alpha\, n(n+1))$ sorted in ascending order.

Further, for any $u, h \in C^1([0, T], \mathbb{R})$ the Gâteaux derivative can be computed analytically. It is noted [23]

$$D_h t_u^n = \lim_{\delta \to 0} \frac{1}{\delta}(t_{u+\delta h}^n - t_u^n)$$

By definition, one has

$$(u + \delta h)^2(t_{u+\delta h}^n) \int_0^{t_{u+\delta h}^n} (u + \delta h)(s)ds = u^2(t_u^n) \int_0^{t_u^n} u(s)ds \tag{17}$$

From this equality, a few lines of calculus give the result, by letting $\delta \to 0$,

$$D_h t_u^n = -\frac{u(t_u^n) \int_0^{t_u^n} h(s)ds + 2h(t_u^n) \int_0^{t_u^n} u(s)ds}{u^2(t_u^n) + 2\dot{u}(t_u^n) \int_0^{t_u^n} u(s)ds}$$

This formulation is valid under the assumptions of the statement. □

Lemma 2. *For any* $n \in 2, ..., N$, *the mappings* $u \mapsto P(t_u^n)$ *and* $u \mapsto x(T) - x(t_u^n)$ *are Gâteaux differentiable at any* u *satisfying the assumptions of Lemma 1 in any direction* $h \in C^1([0, T], \mathbb{R})$.

Proof. Concerning $P(t_u^n)$, the result readily follows as it is the unique solution of Eq. (6) from $t = 0$ to $t = t_u^n$, which, according to Lemma 1 is Gâteaux differentiable. The mapping $x(T) - x(t_u^n)$ is also the result of integration of Eq. (5) which, over the considered interval, boils down to $\dot{f}_n(t) = \lambda_n(t)$, because $t_u^n \geq t_u^2$ from Lemma 1. The right-hand side of this differential equation is smooth. As such, $x(T) - x(t_u^n)$ is Gâteaux differentiable. □

Lemma 3. *The cost function* $\ni u \mapsto J(u)$ *is Gâteaux differentiable at any* u *satisfying the assumptions of Lemma 1 in any direction* $h \in C^1([0, T], \mathbb{R})$

Proof. The cost is written under the form of Problem 2 using smooth mappings of the arguments $P(t_u^n)$, $x(T) - x(t_u^n)$, for $n = 2, \ldots, N$. These arguments are Gâteaux differentiable according to Lemma 2. This yields the conclusion by the chain rule on Gâteaux derivatives, following [24][p. 33]. □

4. Numerical experiments

For illustration, two test-cases from the literature are considered. In both scenarios the noise amplitude is constant for every mode $|\xi_n(0)| = R_0/500$. The initial phases of the modes are uniformly distributed over $[0, 2\pi]$. The number of Fourier modes is $N = 30$.

Test case 1, from [13]. Here $Q = 9.3\,\mathrm{cm^2\,s^{-1}}$, $\eta_1 \approx 0$, $\eta_2 = 5.21\,\mathrm{g\,cm^{-1}\,s^{-1}}$, $b = 0.15\,\mathrm{cm}$, $\sigma = 63\,\mathrm{dynes\,cm^{-1}}$, $(\alpha = 0.0227\,\mathrm{cm^3\,s^{-1}})$, $R_0 = 0.05\,\mathrm{cm}$. The time horizon is set to $T = 30\,\mathrm{s}$.

Test case 2, from [14]. In this scenario $Q = 3.9859\,\mathrm{cm^2\,s^{-1}}$, $\eta_1 \approx 0$, $\eta_2 = 4.85\,\mathrm{g\,cm^{-1}\,s^{-1}}$, $b = 0.1\,\mathrm{cm}$, $\sigma = 25\,\mathrm{dynes\,cm^{-1}}$, $(\alpha = 0.0043\,\mathrm{cm^3\,s^{-1}})$, $R_0 = 0.45\,\mathrm{cm}$. The time horizon is set to $T = 18\,\mathrm{s}$.

In both cases, the OCP (14) is solved by searching a singular point of the cost function J. In practice, the cost function is optimized over a class of smoothed piecewise C^1 functions from $[0, T]$ to $\mathbb{R}$. The constraint $R(T) = R_T$ is automatically satisfied by imposing that every element in this class is such that $\int_0^T u(s)ds = u_0 T$ with $u_0 = \frac{Q}{\pi}$ is a constant defined by the scenario. This is done by considering functions of the type $[0, T] \ni t \mapsto u(t) = u_0 + v(t)$ where v is the smoothed version of a piecewise C^1 and has zero average. In order to guarantee that Lemma 3 holds, v is constrained so that it satisfies Eq. (15).

Dealing with such a class allows one to recast the functional optimization problem into a finite dimensional space, which can be solved using a general SQP technique [25]. In practice, one considers $0 = x_1 \leq \cdots \leq x_m = T$ and solves

$$\begin{aligned} \underset{(c_1, ..., c_m)}{\text{minimize}} \quad & J \\ \text{subject to} \quad & w(t) = \sum_{k=2}^{m} c_{k-1} + (c_k - c_{k-1}) \frac{t - x_{k-1}}{x_k - x_{k-1}} \mathbb{1}_k(t), \\ & u(t) = u_0 + \varphi * w(t) - \int_0^T \varphi * w(t)dt, \\ & |c_k| \leq c_{\max}, \quad k = 1, ..., m, \\ & c_1 + ... + c_m = 0 \end{aligned} \tag{18}$$

where $m > 1$ (typically from $m = 10$ to $m = 20$), $\mathbb{1}_k$ is the indicator function of the semi-open interval $[x_{k-1}, x_k)$ for $k = 2, \ldots, m-1$, and $\mathbb{1}_m$ is the indicator function of $[x_{m-1}, x_m]$, φ is a mollifier in the sense of [26] and $*$ denotes the convolution operator, so that $\varphi * w$ is a smoothed version of w.

First, test case 1 is treated. The results obtained with a constant input signal are given in Fig. 2-(top), with the single-mode optimization model from [14] in Fig. 2-(middle), with the proposed all-modes optimized time varying signal in Fig. 2-(bottom). The magnitudes of the modes are reported in Fig. 3.

Then, test case 2 is treated. The results obtained with a constant input signal are given in Fig. 4-(top), with the single-mode optimization model from [14] in Fig. 4-(middle), with the proposed all-modes optimized time varying signal in Fig. 4-(bottom). The magnitudes of the modes are reported in Fig. 5.

Several observations can be made. In both cases, the proposed optimization procedure produces "sigmoid"-shaped histories for the flowrate Q. Compared to the single-mode optimization model from [14], it suggests to start with stronger initial flowrates and tamed down final values for this variable. The magnitudes of the modes reported in Figs. 3 and 5 are clearly shifted towards the low-frequencies, as a result of the minimization of the all-modes cost function. This phenomenon could be made more visible by using non-uniform weights on the modes in the optimization problem. The cost function is reduced by

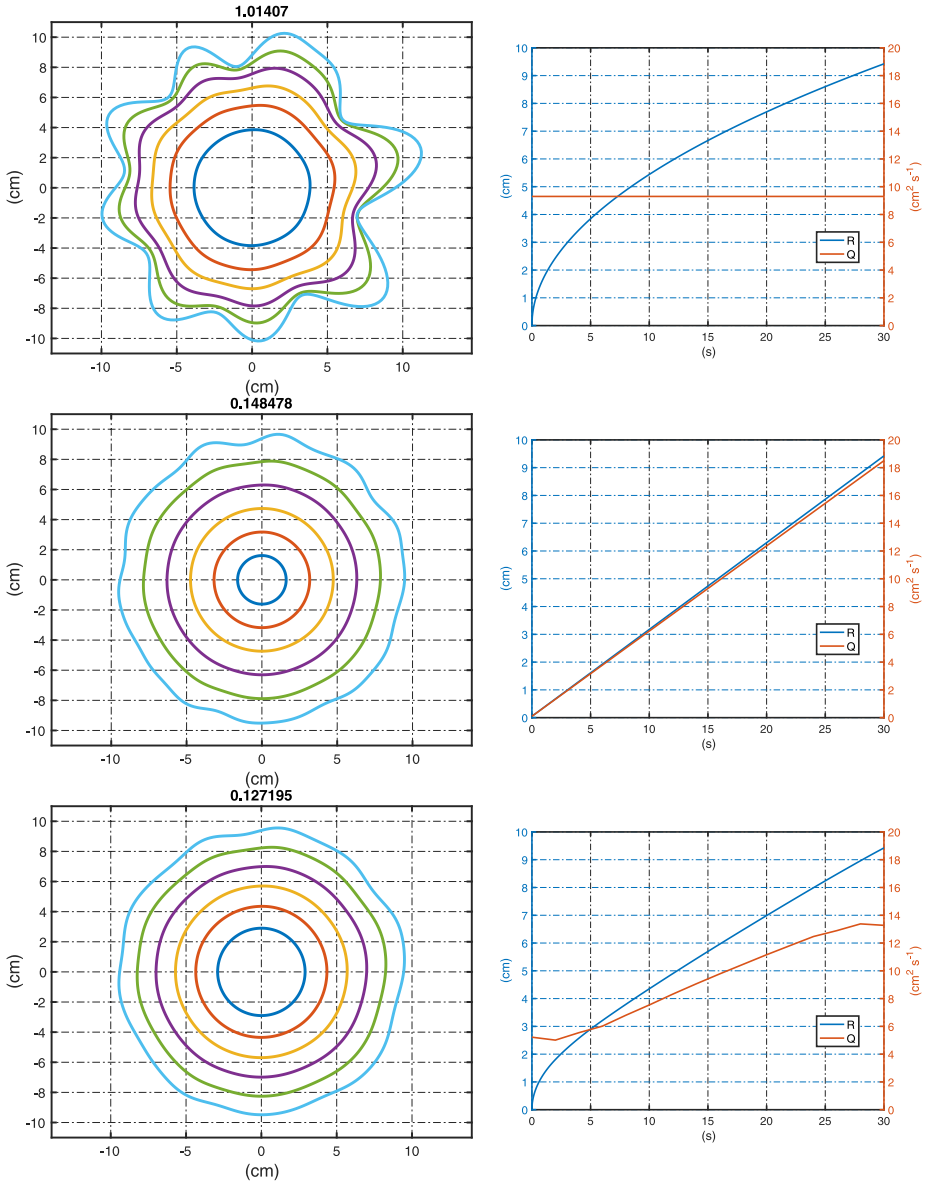

Fig. 2. Behavior for a (top) constant input signal, (middle) time-varying input signal, (bottom) optimized input signal for test case 1 from [13]. The respective values of the cost function are reported as titles on the left plots.

an extra 20% when employing the presented methodology compared to the single-mode method (values are reported in the titles of the left plots in Figs. 2 and 4).

From this, it is believed that the results can be generalized to various other scenarios. How large is the optimality improvement is to be established on a case-by-case basis. Further, it would be instructive to identify the main governing factors. Among the possible culprits are the parameters defining the parameters α, and the time horizon T. In particular it is expected that the larger T is, the more the high frequency modes become important in the problem as they start later and eventually have the time to develop and have a large contribution in the cost function. Thus, it becomes increasingly important to restrain their growth.

5. Conclusion and perspectives

The optimal control problem of viscous fingering is a problem of practical importance. Hindering the formation of fingers is a way to allow a smooth an efficient flow. The results of this article show that the apparent non-smoothness in state-of-the art physical modeling is in fact

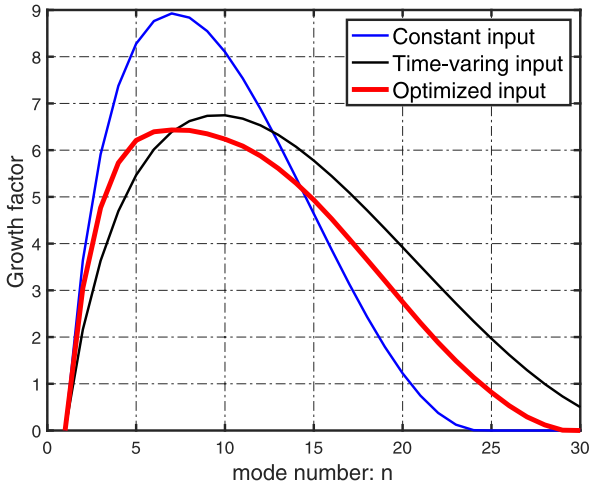

Fig. 3. Growth-rates of the $N = 30$ modes for test case 1 from [13].

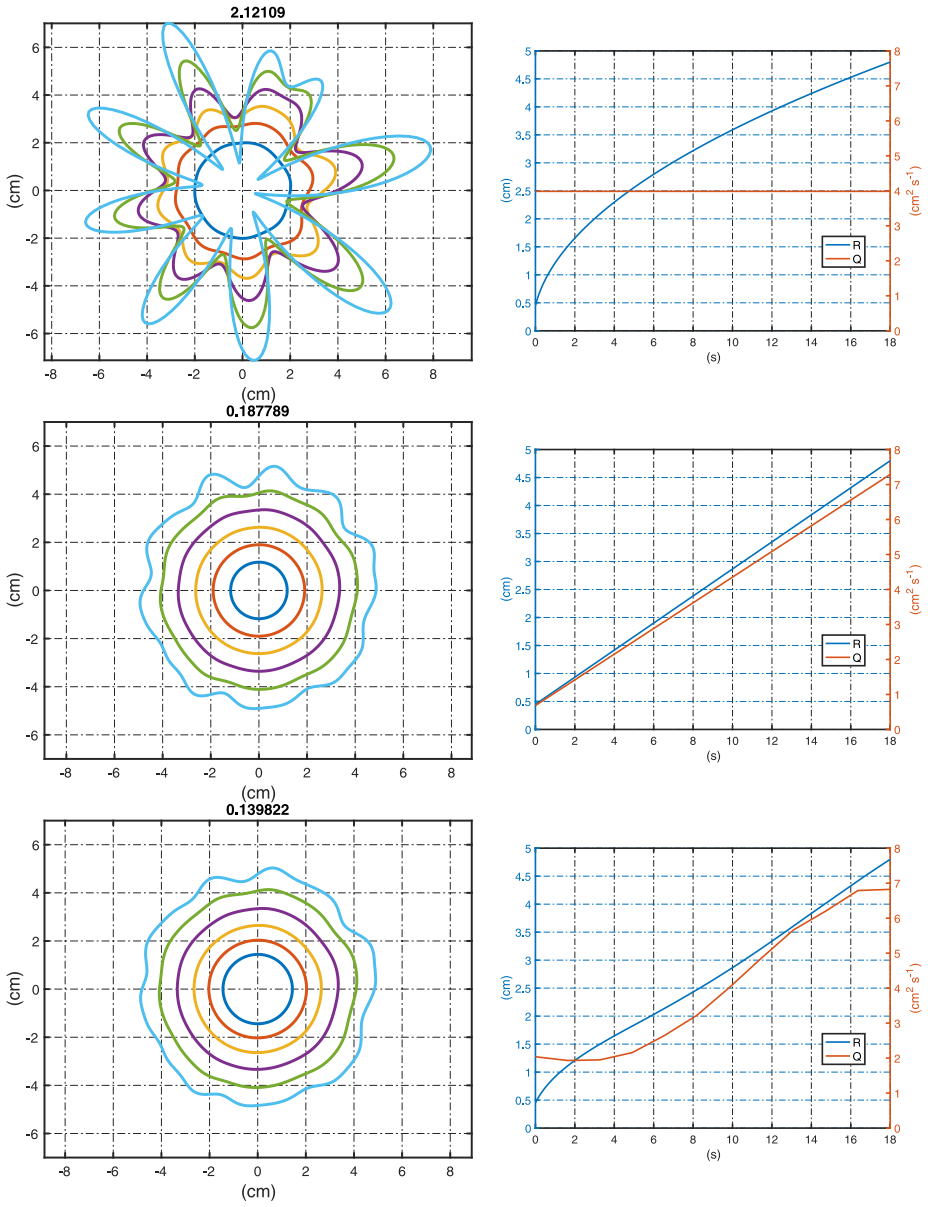

Fig. 4. Behavior for a (top) constant input signal, (middle) time-varying input signal, (bottom) optimized input signal for test case 2 from [14]. The respective values of the cost function are reported as titles on the left plots.

not as troublesome as one might fear from a mathematical viewpoint. This is due to the ease with which the jumps can be mathematically reformulated using prime integrals. Consequently, the inherent nature of any generic optimal control problem for these systems is a multiple stage trajectory optimization problem at times depending implicitly on the control variable. This formulation, Problem 2, has been shown here to be smooth in a mathematical sense and allows one to characterize optimal solutions and to develop methods to numerically estimate them.

In addition to the provided numerical findings, which emphasize that a time-varying flow rate – more encompassing than previously explored in the literature – effectively enhances the roundness of the interface beyond current standards, several avenues for future research are proposed.

Experiments could be conducted to explore the relevance of the presented conclusions further. On the theory side, it would be worth trying to study the controllability of this system. In particular, an open question at this stage is to determine what are the actual shapes for the interface that can be created using varying flowrates over a finite horizon. Besides these open-loop considerations, one very interesting point is to try to develop closed-loop controllers for these systems. A question that one can formulate for future research is the following. Consider the system after a time such that every mode has started to grow, what is the best controller to reach a target shape over the rest of the horizon? Another problem of importance is related to robustness and adaptation to errors in the model. In its formulation, Problem 2 involves only α (and A) as source of uncertainty. Its initial and final conditions are fixed. Possible sources of error in these parameters involves uncertainty in the gap value, the viscosities and surface tension. Over a finite time-horizon it would be valuable to identify possible mismatch in these values and promptly recompute a trajectory. This

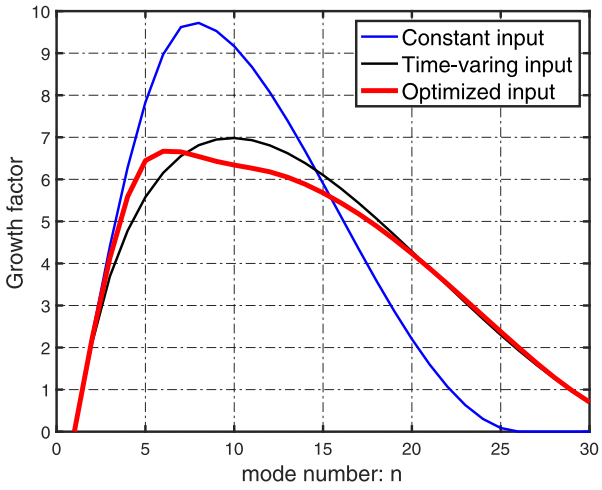

Fig. 5. Growth-rates of the $N = 30$ modes for test case 2 from [14].

underscores the need for the development of rapid trajectory planning methodologies.

Declaration of competing interest

The authors declare that they have no known competing financial interests or personal relationships that could have appeared to influence the work reported in this paper.

Data availability

No data was used for the research described in the article.

References

[1] D. Derks, A. Lindner, C. Creton, D. Bonn, Cohesive failure of thin layers of soft model adhesives under tension, J. Appl. Phys. 93 (3) (2003) 1557–1566.
[2] H. Sarma, Viscous fingering: one of the main factors behind poor flood efficiencies in petroleum reservoirs, Powder Technol. 48 (1) (1986) 39–49.
[3] J.-D. Chen, D. Wilkinson, Pore-scale viscous fingering in porous media, Phys. Rev. Lett. 55 (18) (1985) 1892.
[4] A. Pinilla, M. Asuaje, N. Ratkovich, Experimental and computational advances on the study of viscous fingering: an umbrella review, Heliyon 7 (7) (2021).
[5] T.A. Witten, L.M. Sander, Diffusion-limited aggregation, Phys. Rev. B 27 (1983) 5686–5697.
[6] P.G. Saffman, G.I. Taylor, The penetration of a fluid into a porous medium or Hele-Shaw cell containing a more viscous liquid, Proc R Soc Lond Ser A 245 (1242) (1958) 312–329.
[7] R.L. Chuoke, P. van Meurs, C. van der Poel, The instability of slow, immiscible, viscous liquid-liquid displacements in permeable media, Trans. AIME 216 (01) (1959) 188–194.
[8] D. Bensimon, L.P. Kadanoff, S. Liang, B.I. Shraiman, C. Tang, Viscous flows in two dimensions, Rev. Modern Phys. 58 (1986) 977–999.
[9] S.K. Kabiraj, S. Tarafdar, Finger velocities in the lifting Hele–Shaw cell, Physica A 328 (3) (2003) 305–314.
[10] Z. Zheng, H. Kim, H.A. Stone, Controlling viscous fingering using time-dependent strategies, Phys. Rev. Lett. 115 (17) (2015) 174501.
[11] S. Li, J.S. Lowengrub, J. Fontana, P. Palffy-Muhoray, Control of viscous fingering patterns in a radial Hele-Shaw cell, Phys. Rev. Lett. 102 (17) (2009) 174501–1–4.
[12] L.C. Morrow, T.J. Moroney, S.W. McCue, Numerical investigation of controlling interfacial instabilities in non-standard Hele-Shaw configurations, J. Fluid Mech. 877 (2019) 1063–1097.
[13] J. Miranda, M. Widom, Radial fingering in a Hele-Shaw cell: a weakly nonlinear analysis, Physica D 120 (3) (1998) 315–328.
[14] E.O. Dias, E. Alvarez-Lacalle, M.S. Carvalho, J.A. Miranda, Minimization of viscous fluid fingering: a variational scheme for optimal flow rates, Phys. Rev. Lett. 109 (14) (2012) 144502–1–5.
[15] T. Lins, J. Azaiez, Resonance-like dynamics in radial cyclic injection flows of immiscible fluids in homogeneous porous media, J. Fluid Mech. 819 (2017) 713–729.
[16] E.O. Dias, J.A. Miranda, Control of radial fingering patterns: A weakly nonlinear approach, Phys. Rev. E 81 (1) (2010) 016312.
[17] Í.M. Coutinho, J.A. Miranda, Control of viscous fingering through variable injection rates and time-dependent viscosity fluids: beyond the linear regime, Phys. Rev. E 102 (6) (2020) 063102.
[18] I.M. Gelfand, S.V. Fomin, Calculus of Variations, Dover, 2000.
[19] P. Tabeling, Introduction To Microfluidics, OUP Oxford, 2005.
[20] B.J. Kirby, Micro-and Nanoscale Fluid Mechanics: Transport in Microfluidic Devices, Cambridge University Press, 2010.
[21] S.S.S. Cardoso, A.W. Woods, The formation of drops through viscous instability, J. Fluid Mech. 289 (1995) 351–378.
[22] L.S. Pontryagin, V.G. Boltyanskii, R.V. Gamkrelidze, E.F. Mishchenko, Théorie Mathématique de Processus Optimaux, Editions Mir, Moscou, 1974.
[23] W. Rudin, Functional Analysis International Series in Pure and Applied Mathematics, Tata McGraw-Hill, 1974.
[24] A. Kriegl, P. Michor, The Convenient Setting of Global Analysis, in: Mathematical Surveys, American Mathematical Society, 1997.
[25] J. Nocedal, S.J. Wright, Numerical Optimization, Springer, 1999.
[26] G.B. Folland, Real Analysis: Modern Techniques and their Applications, Vol. 40, John Wiley & Sons, 1999.